

State identification and tunable Kondo effect of MnPc on Ag(001)

Jens Kugel,^{1,*} Michael Karolak,^{2,*} Andreas Krönlein,¹ Jacob Senkpiel,^{1,†} Pin-Jui Hsu,^{1,‡}
Giorgio Sangiovanni,² and Matthias Bode^{1,3}

¹*Physikalisches Institut, Universität Würzburg, Am Hubland, 97074 Würzburg, Germany*

²*Institut für Theoretische Physik und Astrophysik, Universität Würzburg, Am Hubland, 97074 Würzburg, Germany*

³*Wilhelm Conrad Röntgen-Center for Complex Material Systems (RCCM), Universität Würzburg, Am Hubland, D-97074 Würzburg, Germany*

(Received 26 March 2015; revised manuscript received 27 May 2015; published 17 June 2015)

We present a detailed investigation of spectroscopic features located at the central metal ion of MnPc (where Pc represents phthalocyanine) on Ag(001) by means of scanning tunneling spectroscopy (STS) and first-principles theory. STS data taken close to the Fermi level reveal an asymmetric feature that cannot be fitted with a single Fano function representing a one-channel Kondo effect. Instead, our data indicate the existence of a second superimposed feature. Two potential physical origins, a second Kondo channel related to the $d_{xz/yz}$ orbitals, and a spectral feature of the d_{z^2} orbital itself, are discussed. A systematic experimental and theoretical comparison of MnPc with CoPc and FePc indicates that the second feature observed on MnPc is caused by the d_{z^2} orbital. This conclusion is corroborated by STM-induced dehydrogenation experiments on FePc and MnPc which in both cases result in a gradual shift towards more positive binding energies and a narrowing of the Kondo resonance. Theoretical analysis reveals that the latter is caused by the reduced hybridization between the d orbital and the substrate. Spatially resolved differential conductivity maps taken close to the respective peak positions show that the intensity of both features is highest over the central Mn ion, thereby providing further evidence against a second Kondo channel originating from the $d_{xz/yz}$ orbital of the central Mn ion.

DOI: [10.1103/PhysRevB.91.235130](https://doi.org/10.1103/PhysRevB.91.235130)

PACS number(s): 75.70.-i, 75.20.Hr, 68.37.-d, 31.15.-p

I. INTRODUCTION

In recent years intensive research has been carried out to investigate the electronic and magnetic properties, the growth behavior, and the excitations of phthalocyanine molecules, a class of molecules with a planar organic frame and a metal ion at the center [1–10]. Phthalocyanines have attracted much attention due to their extraordinary chemical flexibility, which allows the chemical species of the central metal ion to be varied over a wide range of the periodic table of elements. This flexibility allows the tuning of phthalocyanine molecules towards unique functionalities which, together with their thermal and chemical stability, makes them excellent candidates for future molecular electronic [11,12] or spintronic [13,14] devices.

Since transport properties, which are key for the future design of organic electronic devices, are governed by states close to the Fermi energy E_F , particular attention has been paid to a thorough understanding of the interaction of molecules with surfaces and the resulting electronic properties and density of states around E_F . Especially in the context of molecular spintronics, the Kondo effect [15–17], i.e., the coherent screening of unpaired spins by itinerant conduction electrons of the substrate which leads to a pronounced feature close to the Fermi level, has been intensively studied [1,18,19].

In fact, transition-metal phthalocyanines (TMPc) turned out to exhibit a very rich Kondo behavior. For example, several studies investigated the manipulation of the Kondo effect through conformational switching [20,21], by molecular assembly [22,23], and through the influence of the adsorption site [24,25]. Particular focus was put on the manipulation of the Kondo effect by means of chemical modification. In particular, the controlled removal of up to two hydrogen atoms per pyrrole ring turned out to be a formidable opportunity to modify the adsorption geometry between the molecule and the substrate [1]. Since the interaction of the molecule spin with the substrate conduction electrons is at the heart of the Kondo effect, slight changes in the adsorption geometry can indeed lead to dramatic changes of the Kondo temperature or the line shape [1]. Another method used to manipulate the Kondo effect is charge doping of molecules. This was achieved by the deposition of alkali metals, such as Li, K, or Cs, onto molecular layers [26,27].

It is not always straightforward, however, to model the observed spectroscopic features with the Fano line shape expected from the Kondo effect [28]. As long as different features in the projected density of states are energetically well separated from each other, the identification of different orbitals and their contribution to the electronic properties is usually relatively easy to achieve. The analysis is far more complicated if several electronic states or resonances contribute to or even overlap with the projected density of states, as in the case of MnPc on Ag(001) [29] or on Pb(111) [2]. In both cases the density of states close to the Fermi level is dominated by a Kondo-related peak with a Fano line shape. Close inspection revealed, however, that it is accompanied by a superimposed spectroscopic feature, which in the case of MnPc/Pb(111) was assumed to be a second Kondo channel [2]. The multiorbital nature of these systems makes the understanding of the low-energy physics particularly challenging, since simple

*Corresponding authors: jens.kugel@physik.uni-wuerzburg.de; michael.karolak@physik.uni-wuerzburg.de

†Present address: Max-Planck Institute for Solid State Research, 70569 Stuttgart, Germany.

‡Present address: Institute of Applied Physics and Interdisciplinary Nanoscience Center Hamburg, University of Hamburg, 20355 Hamburg, Germany.

(few-orbital) models are not sufficient and the whole atomic multiplet structure of the d shell has to be taken into account.

Here we present a detailed study to extract the origin of the two superimposed effects observed on the central metal ion of MnPc on Ag(001). It was performed by combined scanning tunneling spectroscopy (STS), *ab initio* density functional theory (DFT), and mapping onto an Anderson impurity model. Comparison of MnPc with CoPc and FePc suggests a systematic shift of the d orbital towards more positive binding energies. The existence of this feature is confirmed by comparative dehydrogenation experiments performed on FePc and MnPc. This manipulation allows the tuning of the coupling of the d orbital to the substrate. Thereby, the Kondo temperature T_K is reduced from $T_K = (135 \pm 25)$ K for the intact MnPc molecule to $T_K = (43 \pm 5)$ K after removing four hydrogen atoms. By mapping the spatial distribution of the two spectroscopic features with the scanning tunneling microscope (STM), we find that they are both located at the central Mn ion of the phthalocyanine molecule. This spatial distribution is in agreement with the theoretically expected shape of the transition-metal d_{z^2} orbital but significantly deviates from what would be expected for a second Kondo $d_{xz/yz}$ screening channel.

II. DETAILS OF REALIZATION

A. Experimental setup and procedures

Sample preparation was carried out in an ultrahigh vacuum (UHV) chamber with a base pressure $p \leq 5 \times 10^{-11}$ mbar. The clean Ag(001) surface was prepared by cycles of Ar⁺ ion sputtering at an ion energy of 500 eV and subsequent annealing up to 800 K. Source materials with 97% MnPc (Strem Chemicals), 96% FePc (Alfa Aesar), and 96% CoPc (Alfa Aesar) were first purified by sublimation in a tube furnace and then degassed for several hours under UHV conditions. Molecules were sublimated from resistively heated crucibles onto the Ag(001) surface kept at room temperature. During evaporation the pressure did not exceed a value of $p = 6 \times 10^{-10}$ mbar.

After preparation, the sample was immediately transferred into a home-built low-temperature scanning tunneling microscope (LT-STM) (operation temperature $T \approx 4.5$ K). For topographic images the LT-STM was operated in the constant-current mode with the bias voltage U applied to the sample. For scanning tunneling spectroscopy (STS) measurements we applied a small bias voltage modulation U_{rms} (frequency $\nu = 811.7$ Hz), such that tunneling differential conductance dI/dU spectra as well as dI/dU maps can be acquired by detecting the first harmonic by means of a lock-in amplifier. For the spectra in a narrow energy range ($-500 \leq U \leq 500$ mV) a modulation voltage of $U_{\text{rms}} = 1$ mV and for spectra in a wider energy range a modulation voltage of $U_{\text{rms}} = 3$ mV was used. To reduce the influence of tip-induced spectroscopic features point spectra of the clean Ag(001) substrate were subtracted from the molecular spectra. The result is labeled “ $\Delta dI/dU$ ” throughout the paper. Raw data for the substrate and molecular spectra can be found in the Supplemental Material ([30], Fig. S1).

B. Theoretical methodology

To explain the basic trends seen in the experimental spectra we applied DFT. Calculations were performed using the projector-augmented-wave-based [31] Vienna *ab initio* simulation package (VASP) [32,33]. The Perdew-Burke-Ernzerhof version of the generalized gradient approximation [34] was used in combination with the van der Waals dispersion correction by Grimme (DFT-D3) [35].

To obtain the geometries of the TMPc on the Ag(100) surface, single molecules on Ag(100) have been modeled using (8×8) surface supercells with a slab thickness of three layers. The crystal structures were relaxed until the forces acting on each atom were smaller than 0.01 eV/Å. For relaxations we used the Γ point in reciprocal space only. The calculations show that all TMPc molecules adsorb at high-symmetry positions continuing the Ag lattice, i.e., their lateral position is in the center of a square of Ag atoms. The same adsorption site was also found in earlier studies for CuPc [25]. In order to simulate the effects of dehydrogenation, the outer hydrogen atoms were removed from the structure of the molecule and the geometry was again relaxed until convergence.

For partial charge density plots the vacuum in the supercell between two periodic images of the system was increased to >25 Å, and the plane-wave cutoff was increased to 800 eV to ensure the proper representation of the wave function in the vacuum. The charge densities were obtained by integrating the states in a window of ± 200 meV around the Fermi level.

To get a clearer picture of the local physics of the transition-metal $3d$ shell we used projected local orbitals (PLOs) to extract Wannier functions. We employed the projection formalism described in detail in Refs. [36,37], which allows for a well-defined mapping of the band structure onto localized Wannier orbitals. We will refer to this methodology as DFT + PLO in what follows. The Wannier orbitals obtained for MnPc on Ag, which were already shown in Ref. [29], retain shapes similar to the atomic $3d$ orbitals and show a rotation with respect to the high-symmetry cubic axes of the substrate as expected from the adsorption geometry. Despite remaining close to their atomic counterparts, some modifications of the orbitals are visible. These stem from hybridization with the organic parts of the molecule, especially with the $2p$ states of the nitrogen atoms close to the transition-metal center.

To gain a deeper understanding of the coupling between structural and electronic degrees of freedom we use a combination of DFT with the Anderson impurity model (AIM), which describes a single correlated impurity coupled to a bath of conduction electrons. Our PLO Wannier construction allows us to set up a description of the molecule within an Anderson model. It can be written in the multiorbital case as

$$\hat{H}_{\text{AIM}} = \sum_{\nu} \varepsilon_{\nu} \hat{c}_{\nu}^{\dagger} \hat{c}_{\nu} + \sum_{vi} (V_{vi} \hat{c}_{\nu}^{\dagger} \hat{d}_i + V_{vi}^{*} \hat{d}_i^{\dagger} \hat{c}_{\nu}) + \sum_{ij} \varepsilon_{ij} \hat{d}_i^{\dagger} \hat{d}_j + \frac{1}{2} \sum_{ijkl} U_{ijkl} \hat{d}_i^{\dagger} \hat{d}_j^{\dagger} \hat{d}_l \hat{d}_k. \quad (1)$$

Here the first term is the spectrum of the (noninteracting) bath which can be diagonalized in some basis indicated by the creation and annihilation operators \hat{c}_{ν} and \hat{c}_{ν}^{\dagger} . The second term encodes hopping processes between the bath and the

impurity states (\hat{d}_i). The energy levels of the bath are given by ε_v and the hybridization parameters V_{vi} give the amplitude for transitions of particles from the bath onto the impurity and vice versa. They comprise what is called the dynamical, i.e., energy-dependent, hybridization. In our case the bath not only consists of the substrate, but also involves the organic parts of the molecule. Finally, the second line of the equation contains the static crystal field of the impurity ε_{ij} and the full local Coulomb interaction U_{ijkl} . Here we identify the transition-metal center of the molecules with the impurity and absorb the rest of the system into the bath. The model was designed and is best suited for the description of d - or f -shell impurities in simple metal hosts and is capable of describing local correlation physics, like the Kondo effect [17,38].

In our treatment the hybridization is given by a continuous energy-dependent function

$$\Delta_{ij}(\omega) = \sum_v \frac{V_{vi} V_{vj}^*}{\omega - \varepsilon_v + i0^+}. \quad (2)$$

Here, we use DFT to obtain the parameters of the Anderson model [Eq. (1)] from first principles. To this end, we compute the Kohn-Sham Green's function using projections $\langle \phi | \psi_K \rangle$ of the Kohn-Sham wave functions $|\psi_K\rangle$ onto localized orbitals $|\phi\rangle$ using the Kohn-Sham eigenenergies ε_K as

$$G_{ij}(\omega) = \sum_K \frac{\langle \phi_i | \psi_K \rangle \langle \psi_K | \phi_j \rangle}{\omega - \varepsilon_K + i0^+}. \quad (3)$$

The hybridization function can then be obtained from the local Green's function $G_{ij}(\omega)$ of the system at hand. The two are related by

$$G_{ij}^{-1}(\omega) = (\omega + i0^+) \delta_{ij} - \varepsilon_{ij} - \Delta_{ij}(\omega), \quad (4)$$

which can be solved to yield

$$\Delta_{ij}(\omega) = -[G_{ij}^{-1}(\omega) + \varepsilon_{ij} - (\omega + i0^+) \delta_{ij}], \quad (5)$$

where ε_{ij} is the static crystal field. To separate the dynamical, i.e., frequency-dependent, hybridization from the static DFT crystal field, we numerically evaluate the limit $\omega \rightarrow \infty$, where $\omega - G_{ij}^{-1}(\omega) \rightarrow \varepsilon_{ij}$. The spectral functions $A(\omega)$ were obtained from the Green's function in Eq. (4) as

$$A_{ij}(\omega) = -\frac{1}{\pi} \text{Im} G_{ij}(\omega). \quad (6)$$

Here we will use the hybridization function as an additional quantity containing information about the local low-energy physics of the transition-metal center of the molecule. It can give hints about the expected trends in the Kondo temperature, for example.

A full study of the Anderson model using the combination of DFT and a many-body impurity solver, which we will refer to as DFT++ [39], for each stage of dehydrogenation, including detailed investigations of the influence of all relevant parameters as presented in Ref. [29], is beyond the scope of the current work. We have, however, performed calculations along these lines for MnPc, to investigate if the local electronic structure undergoes qualitative changes as a consequence of the dehydrogenation process. To solve the local impurity problem we use the continuous-time quantum Monte Carlo (CT-QMC) method [40] implemented within the hybridization

expansion [41]. See Ref. [42] for a review. Within our implementation the Coulomb interaction is treated approximately, including only density-density terms proportional to $\hat{n}_{i\sigma} = \hat{d}_{i\sigma}^\dagger \hat{d}_{i\sigma}$. In this approximation the Coulomb interaction part of the local Hamiltonian can be written as

$$\begin{aligned} \frac{1}{2} \sum_{ijkl} U_{ijkl} \hat{d}_i^\dagger \hat{d}_j^\dagger \hat{d}_l \hat{d}_k &\approx \frac{1}{2} \sum_{i,j,\sigma} U_{ij} \hat{n}_{i,\sigma} \hat{n}_{j,-\sigma} \\ &+ \frac{1}{2} \sum_{i \neq j, \sigma} (U_{ij} - J_{ij}) \hat{n}_{i,\sigma} \hat{n}_{j,\sigma}, \end{aligned}$$

where the matrices U_{ij} and J_{ij} are the density-density terms of the full Coulomb interaction U_{ijkl} . We have used the full Coulomb interaction as obtained from the Slater integrals F^0 , F^2 , and F^4 for $3d$ -shell systems [43]. The numerical values we used were $F^0 = 4.5$ eV, $F^2 = 6.03$ eV, and $F^4 = 3.77$ eV and correspond to the average Coulomb interaction parameters $U = 4.5$ eV and $J = 0.7$ eV that were obtained from *ab initio* calculations for MnPc [44].

C. Terminology

By $A_m(\omega)$ we denote the spectral functions obtained by adding or removing an electron to or from the Wannier orbital m of Mn or Fe. Within the independent electron approximation, i.e., when we show noninteracting (or DFT) cases as in Figs. 2 and 6, the spectral function corresponds to the unoccupied and occupied densities of states for electron addition and removal, respectively. In this case one can identify spectral peaks with “states”, as electrons are removed from or added to infinitely long-lived levels. Interacting many-body (DFT++) spectral functions, as shown in Fig. 9, correspond to transitions between many-body states rather than to single-particle levels [45]. The typical effect of electron-electron interactions can be seen in Fig. 9, where $A_{z^2}(\omega)$ is shown: new low-lying excitations are created while, at the same time, part of the spectral weight is pushed to higher energies. One can, for instance, very clearly identify a Kondo resonance close to the Fermi level, an additional low-lying peak centered around 25 meV, and a third peak at somewhat higher binding energy. In this particular case the latter probably corresponds to the d_{z^2} contribution to the lower Hubbard band.

In this work we are not going to make a direct comparison between these spectral details and the measured STM dI/dU spectra, because the effects of the tunneling transmission are neglected in our calculation. These may profoundly influence the shape of the spectrum, as has been shown in Refs. [44,46]. Instead, we present an analysis based on a fit of the experimental data with a Fano curve for the Kondo peak and an additional superimposed line shape, effectively taking into account the spectral features at higher binding energy mentioned above (see Fig. 1).

In the rest of the paper we will discuss the orbital character of this additional superimposed feature. For the sake of simplicity we will refer to it in a nonspecific way, namely, as an “orbital state.” This name is motivated by the simple classification that can be made on the basis of the DFT spectral functions for the three molecules considered; see Sec. III A, especially Fig. 1.

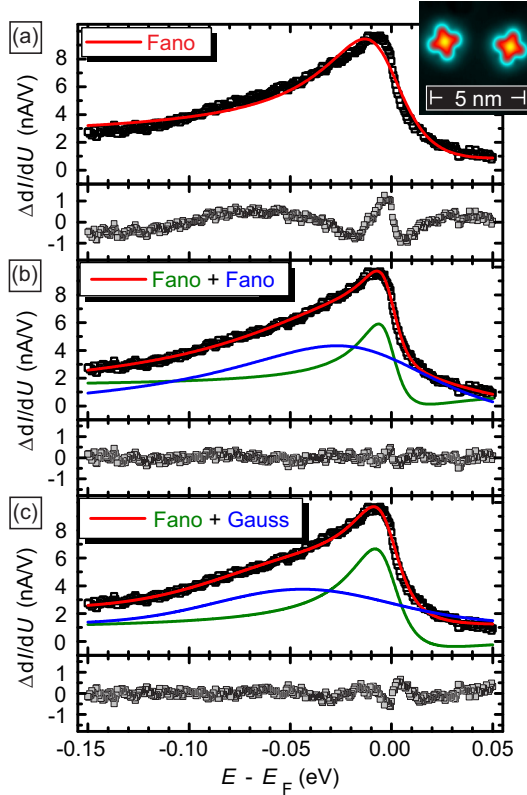


FIG. 1. (Color online) Point spectrum measured with the STM tip positioned over the central metal ion of MnPc (black squares, repeated in the upper panel of each section of this figure) fitted with different functions (stabilization value $U = 0.5$ V, $I = 10$ nA): (a) a single Fano profile for modeling a single Kondo system, (b) two Fano profiles for modeling a double Kondo system, and (c) a Fano profile with a Gaussian peak superimposed for modeling a single Kondo system and a superimposed orbital state. The deviation between the different fitting functions and the measured data is shown in the lower panel (gray squares). While the single Fano profile shows significant deviations from the data, the quality of the fit is greatly improved for the other two models.

III. RESULTS AND DISCUSSION

A. Tunneling spectroscopy of MnPc

The upper panel in Fig. 1(a) shows a typical tunneling spectrum as measured with the STM tip positioned above the central metal ion of MnPc adsorbed on a Ag(001) substrate (black squares). A pronounced spectroscopic feature around the Fermi energy is observed, which we identified as a Kondo screening channel of the d_{z^2} orbital in a previous publication [29]. This spectrum has been fitted with a single Fano profile (red line) [1]

$$\frac{dI}{dU} \propto \frac{(q + \epsilon)^2}{1 + \epsilon^2}, \quad (7)$$

with

$$\epsilon = \frac{eU - \alpha}{\Gamma/2}. \quad (8)$$

Here, q is the interference parameter changing the shape of the resonance, eU is the energy, α describes the energy shift

of the Kondo resonance, and Γ is the width of the resonance:

$$\Gamma = 2\sqrt{(\pi k_B T)^2 + 2(k_B T_K)^2}, \quad (9)$$

where T is the temperature of the sample, k_B the Boltzmann constant, and T_K the Kondo temperature. As can be seen in the lower panel of Fig. 1(a), which shows the difference between the experimental data and the fit, significant deviations are observed, indicating the inadequacy of this model. The shape of the difference curve points towards the existence of another spectroscopic feature that is superimposed on the Fano line and energetically located just below the Fermi energy. Tip effects or surface defects as a reason for the discrepancy can safely be excluded, as—after background subtraction of the Ag(001) spectra—qualitatively similar observations were reproducibly obtained with dozens of different tips and molecules.

In our opinion there are two possible explanations for such a second feature close to the Fermi energy: (i) a second Kondo screening channel, which was, for example, proposed for the same type of molecule, MnPc, adsorbed on Pb(111) [2,47]; or (ii) an orbital state that is energetically close to the d_{z^2} Kondo resonance. Both possibilities were tested by fitting the same data already presented in Fig. 1(a). Figure 1(b) shows a comparison of the two Fano profiles, representing two Kondo screening channels [with Kondo temperatures $T_{K,1} = (84 \pm 15)$ K, $T_{K,2} = (520 \pm 60)$ K]. Correspondingly, in Fig. 1(c) the data were fitted with a superposition of a Fano profile [$T_K = (120 \pm 15)$ K] and a Gaussian function,

$$\frac{dI}{dU} \propto \exp\left(-\frac{(eU - \mu)^2}{2\sigma^2}\right), \quad (10)$$

the latter modeling an orbital state. Here, μ is the position of the center and σ the standard deviation of the Gaussian function. All fit parameters for the aforementioned models of Figs. 1(a)–1(c) are listed in Tables S1 and S2 of the Supplemental Material [30]. As revealed by the very small difference plotted in the lower panels of Figs. 1(b) and 1(c), both models are better suited to describe the experimental data than the single Fano profile used in Fig. 1(a). Due to the subtlety of the variations, however, comparison of the fitting results does not allow a decisive conclusion about which of the two scenarios is the origin of the superimposed effect.

For the analysis presented above, we used Fano profiles, as these functions are most commonly used in the literature to model the spectroscopic features of Kondo resonances probed by STS. Nevertheless, it has been shown that the Frota function [48] can be better suited to fit the Kondo resonance [49]. As the line shape in our analysis is significantly important for our interpretation, the fit was also done with Frota functions instead of Fano profiles. The results are in qualitative agreement and do not change the conclusion of this paper. These fits are listed for clarity in the Supplemental Material ([30], Fig. S2).

B. Comparison with reference molecules

If an orbital state is responsible for the superimposed effect at the central metal ion of MnPc, the most probable d orbitals are the d_{z^2} and the $d_{xz/yz}$ orbitals due to their relatively large overlap with the tip wave functions. Only these d_{\perp} orbitals

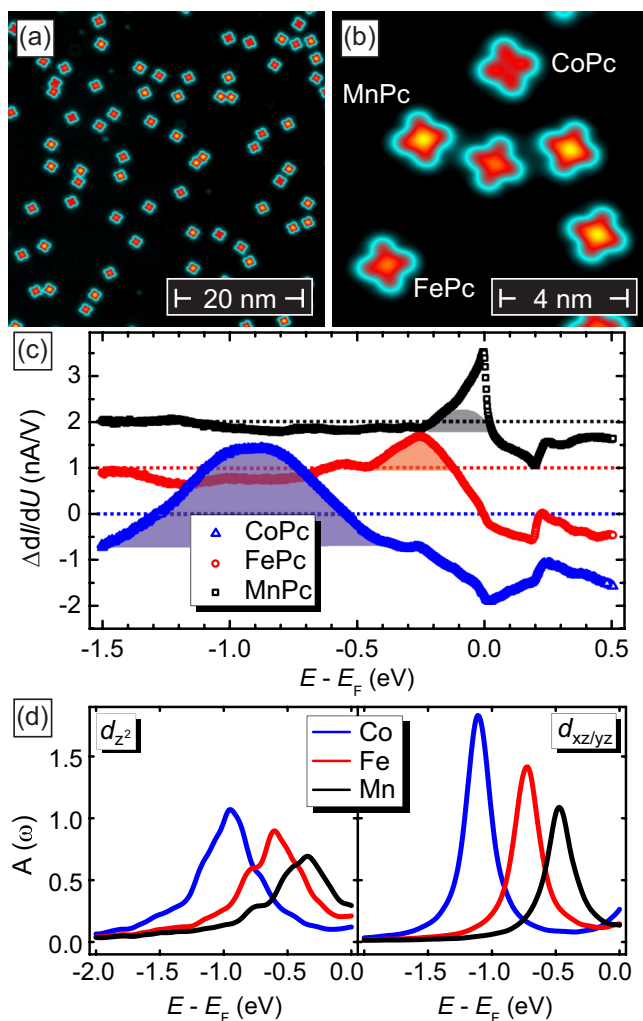


FIG. 2. (Color online) (a), (b) Constant-current topographs of MnPc, FePc, and CoPc on Ag(001) (scan parameters $U = +200$ mV, $I = 1$ nA). (c) Overview spectra of MnPc, FePc, and CoPc taken at the central metal ion of the molecule (stabilization value $U = -1$ V, $I = 1$ nA). The $dI/dU = 0$ intensity for each spectrum is indicated by a colored dashed line. (d) DFT + PLO spectra for CoPc, FePc, and MnPc showing the level shift of d_{z^2} and $d_{xz/yz}$ orbitals.

protrude out of the molecular plane and possess a tunneling probability which may explain the dI/dU signal close to the Fermi energy. To test if these d_{\perp} orbitals are responsible for the second spectroscopic feature close to the Fermi energy, we coevaporated CoPc and FePc as reference molecules together with MnPc. For CoPc and FePc the energetic positions of the orbitals are well known from earlier investigations [50]. Since the d -level occupation gradually decreases when going from CoPc to FePc and eventually to MnPc, we expect a progressive shift of the d orbitals towards the unoccupied states.

Figure 2(a) shows an overview topographic STM image with a surface scan range of 50×50 nm² containing about 70 molecules. The zoomed-in image of Fig. 2(b) reveals that the three TMPc molecules exhibit distinctly different apparent heights. While a pronounced protrusion can be found at the central position of MnPc molecules, the protrusion is less

pronounced for FePc and completely absent for CoPc. A systematic trend is also observed in spectroscopic data taken at the central TM ion of these molecules [Fig. 2(c)]. Here, the d_{\perp} orbitals show up as peaks in the dI/dU spectra and are observed at -0.9 V (blue shaded area) and at -0.25 V (red) for CoPc and FePc, respectively.

These values as well as the position of the interface resonances, energetically located at 0.2 eV, are in excellent agreement with the measurements of Mugarza *et al.* [50]. In the case of MnPc the only state observed in the probed spectroscopic range is the superimposed state located at roughly -0.05 V, as schematically represented by the gray shaded area under the black spectrum in Fig. 2(c). The observed systematic trend for CoPc, FePc, and MnPc, which is in qualitative agreement with our expectations, corroborates our above-mentioned hypothesis that the second feature detected in Fig. 1 is indeed caused by the Mn d_{\perp} orbitals.

The experimentally observed trend of a decreasing binding energy of the d_{\perp} orbitals when going from CoPc to MnPc is in good agreement with the theoretically calculated spectra of molecular $3d$ shells obtained from DFT + PLO calculations that are plotted in Fig. 2(d). These spectra confirm that the d_{z^2} and the $d_{xz/yz}$ orbitals systematically shift as the filling of the d shell decreases. Furthermore, our analysis indicates that the different occupation of the d_{\perp} orbital is also responsible for the different apparent heights obtained in Fig. 2(b) above. These STM data were taken at positive sample bias in order to avoid direct probing of the d_{\perp} orbitals. As the energetic distance of the d_{\perp} orbitals from the Fermi energy decreases, tunneling through the out-of-plane localized d_{\perp} orbitals into the silver surface is enhanced [51] and leads to the appearance of a clearly visible protrusion over the central transition-metal ion of MnPc.

C. Analysis of the spatial distribution

Based on the analysis presented in the last section a d_{\perp} orbital is very likely the origin of the superimposed effect. To ensure that a double Kondo scenario is not responsible for the spectroscopic features close to the Fermi energy, we took a closer look at the spatial distribution of these features. If a double Kondo system were present at the central metal ion of MnPc, two different d orbitals would have to contribute to the dI/dU signal. One obvious choice involves the d_{z^2} and the $d_{xz/yz}$ orbitals, as only these orbitals hybridize strongly enough with the substrate to potentially form a Kondo screening channel [29].

To test if the two d orbitals indeed account for the dI/dU signal close to the Fermi energy, we have performed the measurements presented in Fig. 3. A topographic image of an individual MnPc molecule is shown in Fig. 3(a). Figures 3(b) and 3(c) compare the spatial distribution of the dI/dU signal at $U = -10$ mV, where the main Kondo effect with its Fano profile was observed in MnPc [see the green lines in Fig. 1(b)], with the spatial distribution of the superimposed effect at $U = -50$ mV [see the blue lines in Fig. 1(b)]. The radially averaged experimental data at both energies are shown as red (black) data points in Fig. 3(d). For comparison, theoretically calculated profiles of the d_{z^2} and $d_{xz/yz}$ Wannier orbitals are added as blue and green lines to the graph, respectively. The

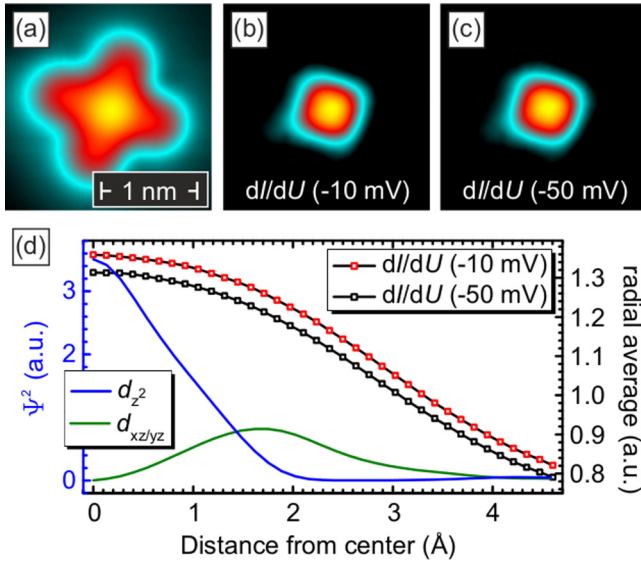


FIG. 3. (Color online) Comparison of the spatial distributions of the two effects close to the Fermi energy: (a) Topography and (b), (c) dI/dU maps of a MnPc molecule measured at the voltages indicated (taken from a full spectroscopy data set, stabilization parameters $U = 200$ mV, $I = 1$ nA). (d) Radial average of these dI/dU maps (data points) compared to a line cut through the square of the calculated Wannier orbitals at 1.5 \AA above the molecule for the d_{z^2} -like orbital (blue) and for the $d_{xz/yz}$ -like orbitals (green) along the respective arm of the molecule where they do not vanish.

sharper drop of the theoretical simulations is due to the neglect of the tip in our calculations. Assuming a tip with a spherical s -orbital tip wave function would lead to a broadening of roughly 5 \AA [52], in good agreement with the experimentally observed result.

In fact, apart from a small offset the two experimental data sets have an almost identical shape. This result provides strong evidence that the second feature close to the Fermi energy is not caused by another Kondo channel originating from the screening of $d_{xz/yz}$ orbitals, but rather from the d_{z^2} orbital of MnPc itself.

D. Dehydrogenation of FePc: Experimental data

To further investigate the superimposed effect we employed the dehydrogenation technique, which was introduced by Zhao and co-workers [1]. In their publication the controlled removal of the outer eight hydrogen atoms from CoPc molecules on Au(111) resulted in a systematic manipulation of the charge state of the molecule and eventually to the appearance of a Kondo resonance absent in pristine molecules. To remove a particular hydrogen atom from the molecule the tip is positioned over the corresponding ligand, the feedback loop is opened, the distance to the arm is increased by roughly 250 pm , and the bias voltage is increased to $(3.2\text{--}3.6) \text{ V}$. The removal of a hydrogen atom is indicated by a sudden characteristic drop in tunneling current [1], which has been interpreted as originating from the arm of the dehydrogenated molecule bending toward the surface.

Figure 4 displays the experimental observations made upon dehydrogenation of FePc which here serves as a reference

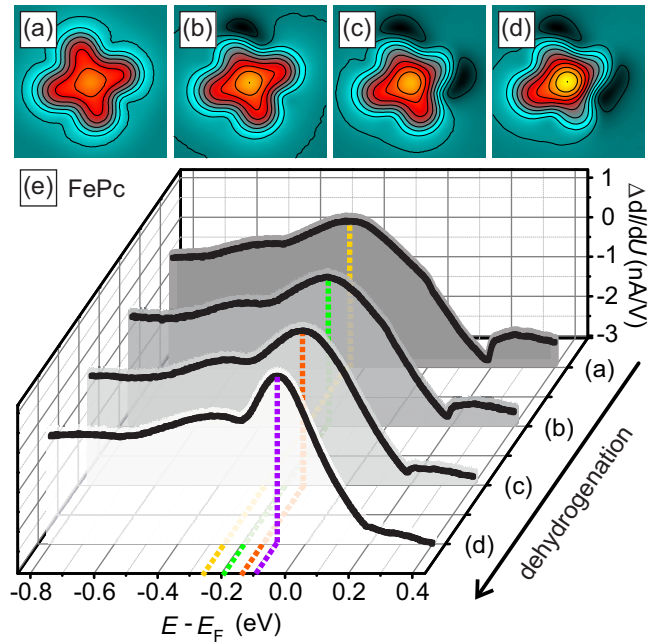


FIG. 4. (Color online) Dehydrogenation series of FePc: (a)–(d) Topographic images of the intact and the partly dehydrogenated molecules. The increment between two contour lines is 15 pm (scan parameters $U = +0.2 \text{ V}$, $I = 1 \text{ nA}$). The dehydrogenated arms can be identified by the deflection of the arms and the resulting charge depletion on the substrate, indicated by the dark area. (e) Series of tunneling spectra (stabilization value $U = -1.0 \text{ V}$, $I = 1 \text{ nA}$) measured on the molecules shown in (a)–(d). A gradual shift of the peak corresponding to the d_{z^2} orbital towards the Fermi level can be observed, as marked by colored dashed lines.

system. While a topographic STM image of the intact molecule is shown in Fig. 4(a), Figs. 4(b)–4(d) show the same molecule after removal of one, two, and three hydrogen atoms, respectively. The associated tunneling spectra measured above the molecule center are plotted as black lines in Fig. 4(e). We have observed five distinct effects:

(i) By looking at the contour lines, which are spaced 15 pm apart, a downwards bending of the dehydrogenated arms can be recognized.

(ii) This bending is accompanied by a very significant reduction of the substrate’s apparent height in close vicinity to the dehydrogenated arm, which appears as a kidney-shaped dark lobe in the images. This effect allows for the most precise determination of the position of the removed hydrogen atom.

(iii) As dehydrogenation progresses the apparent height of the central Fe ion increases, which in Figs. 4(a)–4(d) is indicated by the changing color in the center of the molecule.

(iv) The series of tunneling spectra obtained during this dehydrogenation series of FePc reveals that the width of the peak decreases very significantly from the intact molecule [Fig. 4(a)] all the way to the molecule from which three hydrogen atoms have been removed [Fig. 4(d)].

(v) As the number of removed hydrogen atoms increases we observe a gradual shift of the peak that originates from the d_{z^2} orbital towards the unoccupied states. This trend is highlighted by dashed colored lines in Fig. 4(e) which reveal a

shift of the peak position from $E - E_F = -(250 \pm 10)$ meV for the pristine FePc molecule to $-(90 \pm 5)$ meV after the removal of three hydrogen atoms.

In the following we want to discuss the physical origins and consequences of these effects.

E. Dehydrogenation of FePc and MnPc: DFT + PLO calculations

Observations (i)–(iii) can consistently be described by the theoretical data presented in Fig. 5. The downwards bending of the partly dehydrogenated arms can be nicely reproduced by structural relaxations within DFT, as shown in Fig. 5(a) by comparison of a complete molecule (top left panel) with molecules from which two, four, or eight outer hydrogen atoms have been removed (labeled $-2H$, $-4H$, and $-8H$ hereafter). Although Fig. 5 presents results for MnPc, the results for FePc are qualitatively identical. In our calculations the dehydrogenation was performed starting from the complete molecule and successively removing the outer hydrogen atoms one by one, performing a full structural relaxation at each step, with the same convergence criterion and setup detailed earlier.

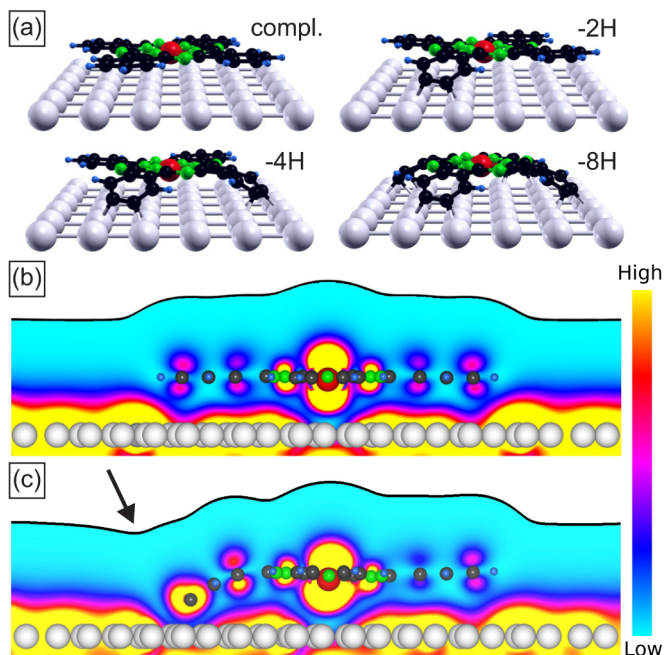


FIG. 5. (Color online) (a) Calculated geometries for the complete MnPc molecule on Ag(001) and for successive dehydrogenation steps with two, four, and eight of the outer hydrogen atoms removed. (b), (c) Charge density of MnPc on Ag(001) integrated over an energy range of ± 200 meV around the Fermi energy, cut along the center of one arm of the molecule for the complete molecule (b) and for the molecule with two outer hydrogens removed (c). The outer surface of the density is an isosurface at $5 \times 10^{-6} e/a_0^3$ (a_0 denoting the Bohr radius), while the color-coded section is cyan-magenta-yellow with yellow being the most saturated at $0.01 e/a_0^3$ descending to cyan at $5 \times 10^{-6} e/a_0^3$. The outer isosurface has been highlighted with a black line to increase visibility. The observed decrease of the charge density in the vicinity of the dehydrogenated arms [compare the left arm of the molecule in (b) and (c)] is in accordance with the reduction of the apparent height observed in the STM topography (cf. Fig. 4).

TABLE I. Summary of theoretical data for the complete and dehydrogenated FePc and MnPc molecules, showing the height of the central atom above the substrate, δz , the filling of the $3d$ shell N_{3d} (obtained from integrating the DFT + PLO spectra), and the value of the hybridization function at the Fermi level where $\Gamma_d = -\text{Im}\Delta(\omega = 0)$.

	Complete	$-2H$	$-4H$	$-8H$
$\delta z(\text{Fe-Ag})$ (\AA)	2.56	2.65	2.72	2.94
$\delta z(\text{Mn-Ag})$ (\AA)	2.50	2.59	2.66	2.87
$N_{3d}(\text{Fe})$	6.7	6.5	6.4	6.3
$N_{3d}(\text{Mn})$	5.2	5.3	5.3	5.3
$\Gamma_d(\text{Fe})$ (eV)	0.69	0.50	0.41	0.31
$\Gamma_d(\text{Mn})$ (eV)	0.73	0.65	0.55	0.40

Hand in hand with this structural relaxation goes an Ag $4s$ charge redistribution of the substrate atoms that participate in the bond to the molecular arm. It is mainly driven by the stronger hybridization between the Ag $4s$ and the C sp orbitals. According to our calculations the Ag $4s$ density of states at the Fermi level drops to about half the value as compared to an equivalent Ag atom placed under a nondehydrogenated arm of the molecule. This drop of the substrate's charge density is nicely visible in Fig. 5(b). Please note that the reduction of the resulting vacuum charge density is strongest at a lateral position slightly away from the molecule [see the arrow in Fig. 5(b)], in agreement with the experimental observations made in Figs. 4(b)–4(d).

Table I summarizes some key results for FePc and MnPc obtained by DFT. The data reveal that progressive dehydrogenation leads to an increasing surface-Fe distance δz . Loosely speaking, observation (iii), i.e., the increasing apparent height of the central Fe ion, appears to be a side effect of the dehydrogenation-induced bending of the molecule. At the same time the total filling of the $3d$ shell, N_{3d} , is reduced. Furthermore, as a consequence of the increased surface-Fe distance the hybridization between the molecular Fe d_{z^2} orbital and the substrate's itinerant conduction electrons changes significantly. In order to model this behavior theoretically, we use the value of the (imaginary part of the) hybridization function Γ_d at the Fermi level as a measure to quantify the coupling. This approximation is valid here since both the hybridization function of the d_{z^2} orbital and the Ag sp density of states are relatively flat in the energy region of interest [29,53]. It is exactly this reduction of the hybridization with the Ag conduction electrons which causes the decreasing width of the Fe d_{z^2} orbital [observation (iv)].

Our DFT calculations can also shed light on the results of STS experiments during dehydrogenation on FePc. As detailed above, in the case of FePc we observe a shift of the d_{z^2} orbital towards the Fermi level [see Fig. 4(e)]. The DFT results presented in Fig. 6(a) show that both the d_{z^2} (left panel) and the $d_{xz/yz}$ orbitals (right) successively shift their spectral weight towards positive binding energies. Qualitatively similar trends are observed in Fig. 6(b) by DFT for MnPc although the states are closer to the Fermi level.

In a simple model of the Kondo effect, i.e., the one-band case with a flat bath [17,54], the Kondo temperature T_K is

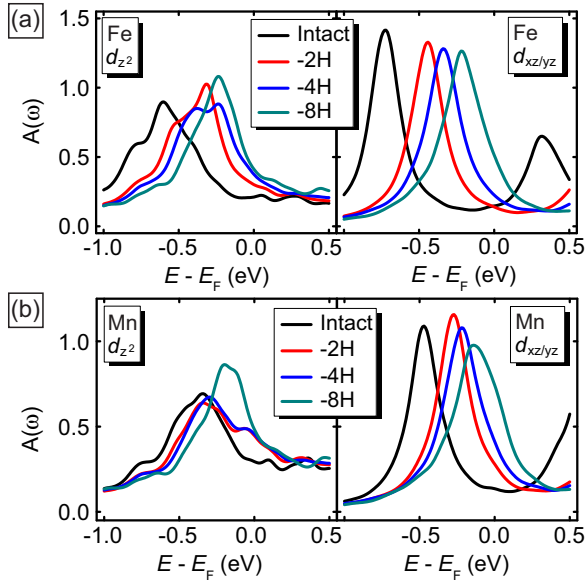


FIG. 6. (Color online) Local spectral functions as obtained from DFT + PLO calculations of the d_{z^2} (left panel) as well as the $d_{xz/yz}$ orbitals (right) for (a) FePc and (b) MnPc, respectively. In both cases a shift of the orbitals towards positive energies is observed. Since the four fold symmetry of $d_{xz/yz}$ orbitals is broken for the $-2H$ and $-4H$ structures, an average is shown.

given by the following formula:

$$k_B T_K = \frac{\sqrt{\Gamma_d U}}{2} \exp\left(\frac{\pi \varepsilon (\varepsilon + U)}{\Gamma_d U}\right), \quad (11)$$

where U is the Coulomb repulsion energy between singly and doubly occupied states, ε is the energetic level of the singly occupied state, and Γ_d is the substrate-induced broadening of these states. In fact, our results obtained on FePc show that the dehydrogenation process leads to a reduced width of the d_{z^2} orbital and reduced occupation N_{3d} . While FePc does not exhibit a Kondo effect at temperatures accessible in our experimental setup, we have shown above that the Kondo temperature of MnPc is relatively high [$T_K = (120 \pm 15)$ K]. If we assume that qualitatively similar trends apply for the hybridization and occupation during dehydrogenation of MnPc, we expect a significant decrease of the Kondo temperature of the dehydrogenated MnPc molecule.

F. Dehydrogenation of MnPc: Experiment and analysis of many-body effects

Indeed, the data taken during the dehydrogenation series of MnPc in Fig. 7 verify this expectation. Again, Figs. 7(a)–7(d) show topographic STM images of the intact molecule and after successive dehydrogenation steps. The corresponding tunneling spectra measured above the molecule center are shown in Fig. 7(e). Fitting the data with a Fano and a Gaussian function that represent the Kondo and the orbital state, respectively, reveals that with successive dehydrogenation the same two effects on the orbital state can be observed as for FePc: it shifts towards the unoccupied states (see the colored hatched lines) and it becomes narrower. Correspondingly, starting from the intact molecule with $T_K = (135 \pm 25)$ K,

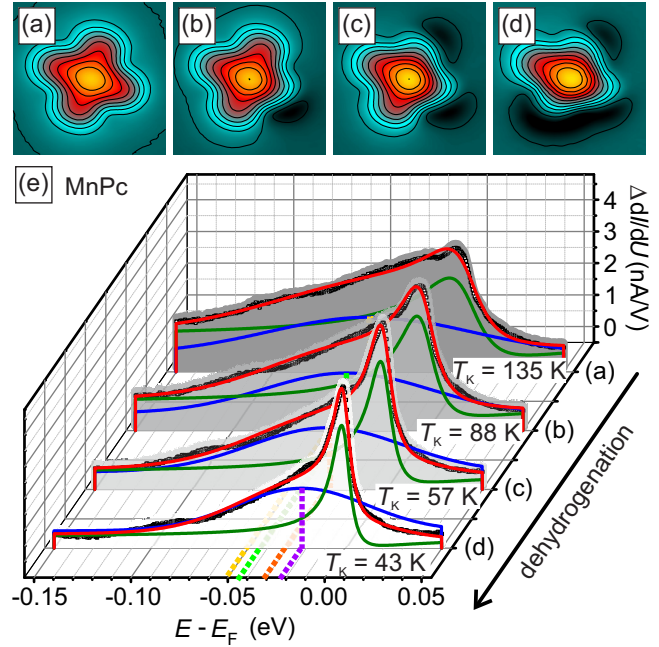


FIG. 7. (Color online) Dehydrogenation series of MnPc: (a)–(d) Topographic images of the intact and the partly dehydrogenated molecules, where the distance between two contour lines is 15 pm (scan parameters $U = +0.2$ V, $I = 1$ nA). (e) The spectroscopy data (black dots) are fitted by a superposition (red) of a Gaussian (blue) and a Fano (green) profile (stabilization value $U = 0.2$ V, $I = 1$ nA). With progressing dehydrogenation a reduction of the Kondo temperature from $T_K = (135 \pm 25)$ K down to $T_K = (43 \pm 5)$ K is observed. The peak positions of the superimposed state are marked by colored dashed lines.

the Kondo temperature is reduced down to $T_K = (43 \pm 5)$ K after the third pulse, with a total of four hydrogen atoms removed. These observations corroborate that the Kondo effect originates from the coherent screening of the transition-metal d_{z^2} orbital.

In the simulations the same behavior as for FePc is observed, albeit somewhat weaker. The spectrum of the d_{z^2} orbital, as well as of the $d_{xz/yz}$ orbitals, show a shift towards the Fermi level; see Fig. 6(b). Also the hybridization function is gradually reduced as indicated in Table I. The charge of the Mn $3d$ shell, however, remains relatively stable over the whole dehydrogenation series, and also the position of the d_{z^2} orbital is not greatly changed. We thus attribute the reduction of the Kondo temperature mostly to the reduction of the hybridization with the silver substrate. Since the Kondo temperature depends exponentially on the hybridization strength, i.e., the broadening Γ_d in Eq. (11), as well as on the level position, small changes can have dramatic effects.

To illustrate this, we have estimated the ratio of Kondo temperatures using Eq. (11) for the symmetric one-band case with $U = 4$ eV, $\varepsilon = -U/2$, and the calculated values of the hybridization from Table I. This particular set of parameters gives Kondo temperatures in the range found in the experiment. Let us stress that while this one-band picture gives an idea of the relevant physical mechanism

at the basis of the Kondo temperature reduction, it is by no means intended to describe the complex physics of the full Mn $3d$ shell. For the two different values of Γ_d for the complete and the -2H and -4H cases with differences $\Delta\Gamma_d = |\Gamma_d^{(1)} - \Gamma_d^{(2)}| = 0.08$ eV and 0.18 eV, respectively, the ratio of the resulting Kondo temperatures is already ~ 1.8 and ~ 4.7 . The observed reduction of the hybridization alone could thus account for the observed change in the Kondo temperatures.

In order to further confirm our physical interpretation of the results, we have performed many-body CT-QMC calculations for the whole Mn $3d$ shell, for each dehydrogenation step. In this way we can directly see how strongly the dehydrogenation alters the many-body excitations. To fix the filling of the Mn $3d$ shell we used the fully localized limit formula [55] for the double-counting correction without further adjustments. This led to a filling between 5.5 and 5.6 electrons for the series. An investigation of the effect of filling on the Kondo effect in MnPc is given in Ref. [29]. Calculations were performed at $T = 116$ K ($\beta = 100$ eV $^{-1}$), i.e., close to the Kondo temperature of the complete molecule, but above the Kondo temperatures of the dehydrogenated molecules. The hybridization expansion CT-QMC solver allows for an analysis of the local eigenstates contributing to the partition function during the imaginary-time evolution [42].

A comparison of these contributions for the dehydrogenation series shows that the main contributions to the partition function remain unchanged. However, some redistribution of weight is observed (see Fig. 8). We identified different realizations of the d^4 , d^5 , and d^6 states as the most important ones for the low-energy physics of the Mn d shell in MnPc. Due to the increased filling ($N_{3d} \sim 5.5$), as compared with the discussion in Ref. [29], now the dominant contributions are the $d^5, S = 3/2$, and $d^6, S = 2$ states. This remains true for the complete molecule as well as for the dehydrogenation series with only minor changes in the respective weights of the states. Appreciable changes are observed for the molecule with four and eight removed hydrogens, which is expected due to the increasing changes in structure and hybridization of the molecule. Upon removing four or more hydrogen atoms an increase of the $S = 2$ and $S = 3/2$ contributions is observed, leading to an increase of the average total spin of the Mn $3d$ shell. This increase comes about mainly as a reduction of the low-spin $S = 0$ and $S = 1/2$ contributions. Upon decoupling the molecule from the surface, a more pronounced “molecular limit” behavior is expected. The latter is characterized by Hund’s rule processes, which dominate over low-spin ones. We thus conclude that the reduced Kondo temperature observed in the experiment is brought about mainly by the modifications of the hybridization function and not by a qualitative change of the ground-state configuration.

Finally, we have calculated the spectra of the intact and dehydrogenated -4H MnPc molecules on Ag(001) within a CT-QMC calculation using the parameters stated above and a temperature of $\beta = 200$ eV $^{-1} \approx 58$ K. The spectra were obtained from the imaginary-time Green’s function via the maximum entropy method [56]. The result for the d_{z^2} orbital is shown in Fig. 9. In our calculation the “orbital state” seen in the STM measurement is made up of a secondary feature next to the Kondo peak that exists outside the Kondo scale

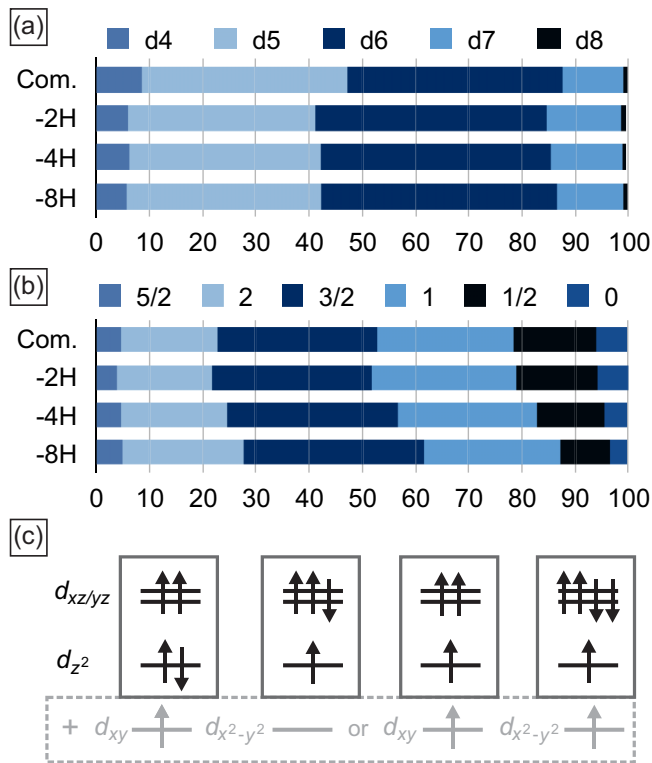


FIG. 8. (Color online) Decomposition of the local eigenstates contributing to the partition function during the CT-QMC imaginary-time evolution (in %) by (a) total charge and (b) total spin of the state. Numbers missing to make up 100% are due to minor contributions of other states. The most probable local contributions remain unaltered during the dehydrogenation series and are shown pictorially in (c).

of the system and a broader peak at higher binding energy, which most likely corresponds to the d_{z^2} contribution to the lower Hubbard band. The same sequence of features is observed for the dehydrogenated molecule as well, although the intensities and positions somewhat differ. Even though

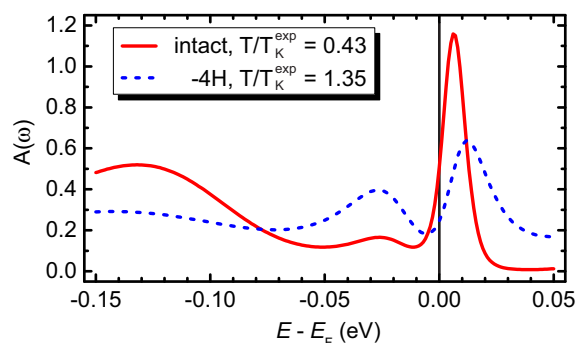


FIG. 9. (Color online) DFT + CT-QMC spectrum of the d_{z^2} orbital for the intact MnPc molecule as well as the -4H molecule on Ag(001). The calculations were performed at $\beta = 200$ eV $^{-1} \approx 58$ K. The curves are labeled by the ratio of the calculated temperature to the experimental Kondo temperature. In both cases, below the Kondo peak, or below its precursor slightly above the Fermi level for the -4H case, we find a small broad peak, which could be the origin of the superimposed feature seen in the STM measurements.

a one-to-one correspondence is beyond the present analysis our calculations corroborate the experimental finding that the broader secondary spectral feature close to the Kondo peak has Mn d_{z^2} orbital character.

IV. CONCLUSIONS

In summary, the identification of two superimposed effects on the central metal ion of MnPc, which are located close to the Fermi energy, was studied by means of scanning tunneling spectroscopy and microscopy and first-principles theory. We compared the spatial distribution of these states by analyzing the energetic level of the d_{z^2} orbitals between different TMPc molecules and by manipulating FePc, as a reference system,

and MnPc, as the system of interest. As a result the two features could be identified as the Kondo resonance of the d_{z^2} orbital and a secondary spectral feature originating in the same orbital. Furthermore, application of the dehydrogenation technique allowed us to tune the Kondo temperature of MnPc by changing the hybridization of the central metal ion with the substrate, while leaving the charge state of the d orbital almost unaffected.

ACKNOWLEDGMENTS

This work has been funded by the Deutsche Forschungsgemeinschaft (DFG) via FOR Grant No. 1162. G.S. acknowledges DFG FOR Grant No. 1346.

-
- [1] A. Zhao, Q. Li, L. Chen, H. Xiang, W. Wang, S. Pan, B. Wang, X. Xiao, J. Yang, J. G. Hou *et al.*, *Science* **309**, 1542 (2005).
- [2] K. J. Franke, G. Schulze, and J. I. Pascual, *Science* **332**, 940 (2011).
- [3] A. Stróżecka, M. Soriano, J. I. Pascual, and J. J. Palacios, *Phys. Rev. Lett.* **109**, 147202 (2012).
- [4] O. I. Arillo-Flores, M. M. Fadlallah, C. Schuster, U. Eckern, and A. H. Romero, *Phys. Rev. B* **87**, 165115 (2013).
- [5] C. Uhlmann, I. Swart, and J. Repp, *Nano Lett.* **13**, 777 (2013).
- [6] T. Sonleitner, I. Swart, N. Pavliček, A. Pöllmann, and J. Repp, *Phys. Rev. Lett.* **107**, 186103 (2011).
- [7] P. Järvinen, S. K. Hämäläinen, M. Ijäs, A. Harju, and P. Liljeroth, *J. Phys. Chem. C* **118**, 13320 (2014).
- [8] Y.-S. Fu, Q.-K. Xue, and R. Wiesendanger, *Phys. Rev. Lett.* **108**, 087203 (2012).
- [9] D. Hao, C. Song, Y. Ning, Y. Wang, L. Wang, X.-C. Ma, X. Chen, and Q.-K. Xue, *J. Chem. Phys.* **134**, 154703 (2011).
- [10] F. Schulz, M. Ijäs, R. Drost, S. K. Hämäläinen, A. Harju, A. P. Seitsonen, and P. Liljeroth, *Nat. Phys.* **11**, 229 (2015).
- [11] J. R. Heath and M. A. Ratner, *Phys. Today* **56**(5), 43 (2003).
- [12] G. Cunibert, G. Fags, and K. Richter, *Introducing Molecular Electronics* (Springer, Berlin, Heidelberg, 2005).
- [13] I. Žutić, J. Fabian, and S. D. Sarma, *Rev. Mod. Phys.* **76**, 323 (2004).
- [14] L. Bogani and W. Wernsdorfer, *Nat. Mater.* **7**, 179 (2008).
- [15] G. D. Scott and D. Natelson, *ACS Nano* **4**, 3560 (2010).
- [16] J. Kondo, *Prog. Theor. Phys.* **32**, 37 (1964).
- [17] H. Hewson, *The Kondo Problem to Heavy Fermions* (Cambridge University Press, Cambridge, 1997).
- [18] W. Liang, M. P. Shores, M. Bockrath, J. R. Long, and H. Park, *Nature (London)* **417**, 725 (2002).
- [19] L. H. Yu, Z. K. Keane, J. W. Cizek, L. Cheng, J. M. Tour, T. Baruah, M. R. Pederson, and D. Natelson, *Phys. Rev. Lett.* **95**, 256803 (2005).
- [20] V. Iancu, A. Deshpande, and S.-W. Hla, *Nano Lett.* **6**, 820 (2006).
- [21] T. Choi, S. Bedwani, A. Rochefort, C.-Y. Chen, A. J. Epstein, and J. A. Gupta, *Nano Lett.* **10**, 4175 (2010).
- [22] V. Iancu, A. Deshpande, and S.-W. Hla, *Phys. Rev. Lett.* **97**, 266603 (2006).
- [23] N. Tsukahara, S. Shiraki, S. Itou, N. Ohta, N. Takagi, and M. Kawai, *Phys. Rev. Lett.* **106**, 187201 (2011).
- [24] E. Minamitani, N. Tsukahara, D. Matsunaka, Y. Kim, N. Takagi, and M. Kawai, *Phys. Rev. Lett.* **109**, 086602 (2012).
- [25] A. Mugarza, N. Lorente, P. Ordejón, C. Krull, S. Stepanow, M.-L. Bocquet, J. Fraxedas, G. Ceballos, and P. Gambardella, *Phys. Rev. Lett.* **105**, 115702 (2010).
- [26] R. Robles, N. Lorente, H. Ishiki, J. Liu, K. Katoh, B. K. Breedlove, M. Yamashita, and T. Komeda, *Nano Lett.* **12**, 3609 (2012).
- [27] C. Krull, R. Robles, A. Mugarza, and P. Gambardella, *Nat. Mater.* **12**, 337 (2013).
- [28] V. Madhavan, W. Chen, T. Jamneala, M. F. Crommie, and N. S. Wingreen, *Science* **280**, 567 (1998).
- [29] J. Kügel, M. Karolak, J. Senkpiel, P.-J. Hsu, G. Sangiovanni, and M. Bode, *Nano Lett.* **14**, 3895 (2014).
- [30] See Supplemental Material at <http://link.aps.org/supplemental/10.1103/PhysRevB.91.235130> for further details on the experiments and for additional experimental data sets.
- [31] P. E. Blöchl, *Phys. Rev. B* **50**, 17953 (1994).
- [32] G. Kresse and J. Hafner, *J. Phys.: Condens. Matter* **6**, 8245 (1994).
- [33] G. Kresse and D. Joubert, *Phys. Rev. B* **59**, 1758 (1999).
- [34] J. P. Perdew, K. Burke, and M. Ernzerhof, *Phys. Rev. Lett.* **77**, 3865 (1996).
- [35] S. Grimme, *J. Comput. Chem.* **27**, 1787 (2006).
- [36] B. Amadon, F. Lechermann, A. Georges, F. Jollet, T. O. Wehling, and A. I. Lichtenstein, *Phys. Rev. B* **77**, 205112 (2008).
- [37] M. Karolak, T. O. Wehling, F. Lechermann, and A. I. Lichtenstein, *J. Phys.: Condens. Matter* **23**, 085601 (2011).
- [38] J. R. Schrieffer and P. A. Wolff, *Phys. Rev.* **149**, 491 (1966).
- [39] A. I. Lichtenstein and M. I. Katsnelson, *Phys. Rev. B* **57**, 6884 (1998).
- [40] A. N. Rubtsov, V. V. Savkin, and A. I. Lichtenstein, *Phys. Rev. B* **72**, 035122 (2005).
- [41] P. Werner, A. Comanac, L. de' Medici, M. Troyer, and A. J. Millis, *Phys. Rev. Lett.* **97**, 076405 (2006).
- [42] E. Gull, A. J. Millis, A. I. Lichtenstein, A. N. Rubtsov, M. Troyer, and P. Werner, *Rev. Mod. Phys.* **83**, 349 (2011).
- [43] J. C. Slater, *Quantum Theory of Atomic Structure* (McGraw-Hill, New York, 1960), Vol. 1.
- [44] D. Jacob, M. Soriano, and J. J. Palacios, *Phys. Rev. B* **88**, 134417 (2013).
- [45] A. L. Fetter and J. D. Walecka, *Quantum Theory of Many-Particle Systems* (Dover Publications, New York, 2003).
- [46] M. Buongiorno Nardelli, *Phys. Rev. B* **60**, 7828 (1999).

- [47] J. Bauer, J. I. Pascual, and K. J. Franke, *Phys. Rev. B* **87**, 075125 (2013).
- [48] H. O. Frota, *Phys. Rev. B* **45**, 1096 (1992).
- [49] H. Prüser, M. Wenderoth, P. E. Dargel, A. Weismann, R. Peters, T. Pruschke, and R. G. Ulbrich, *Nat. Phys.* **7**, 203 (2011).
- [50] A. Mugarza, R. Robles, C. Krull, R. Korytár, N. Lorente, and P. Gambardella, *Phys. Rev. B* **85**, 155437 (2012).
- [51] X. Lu and K. W. Hipps, *J. Phys. Chem. B* **101**, 5391 (1997).
- [52] J. Tersoff and D. R. Hamann, *Phys. Rev. Lett.* **50**, 1998 (1983).
- [53] S. Gardonio, M. Karolak, T. O. Wehling, L. Petaccia, S. Lizzit, A. Goldoni, A. I. Lichtenstein, and C. Carbone, *Phys. Rev. Lett.* **110**, 186404 (2013).
- [54] F. D. M. Haldane, *Phys. Rev. Lett.* **40**, 416 (1978).
- [55] M. T. Czyżyk and G. A. Sawatzky, *Phys. Rev. B* **49**, 14211 (1994).
- [56] M. Jarrell and J. E. Gubernatis, *Phys. Rep.* **269**, 133 (1996).